Supporting Information

Boosting the maximized output energy density of triboelectric nanogenerator

Ru Guo[1], Xin Xia[2], Hang Luo[5], Dou Zhang[5], Yunlong Zi*[1,2.3,4]

1 Department of Mechanical and Automation Engineering, The Chinese University of Hong Kong, Shatin, N.T. Hong Kong, China

2 Thrust of Sustainable Energy and Environment, The Hong Kong University of Science and Technology (Guangzhou), Nansha, Guangzhou, Guangdong, 511400, China

3 HKUST Shenzhen-Hong Kong Collaborative Innovation Research Institute, Futian, Shenzhen, Guangdong, 518048, China

4 Guangzhou HKUST Fok Ying Tung Research Institute, Nansha, Guangzhou, Guangdong 511457, China

5 Powder Metallurgy Research Institute, State Key Laboratory of Powder Metallurgy, Central South University, Changsha, 410083, Hunan Province, China

E-mail: ylzi@hkust-gz.edu.cn

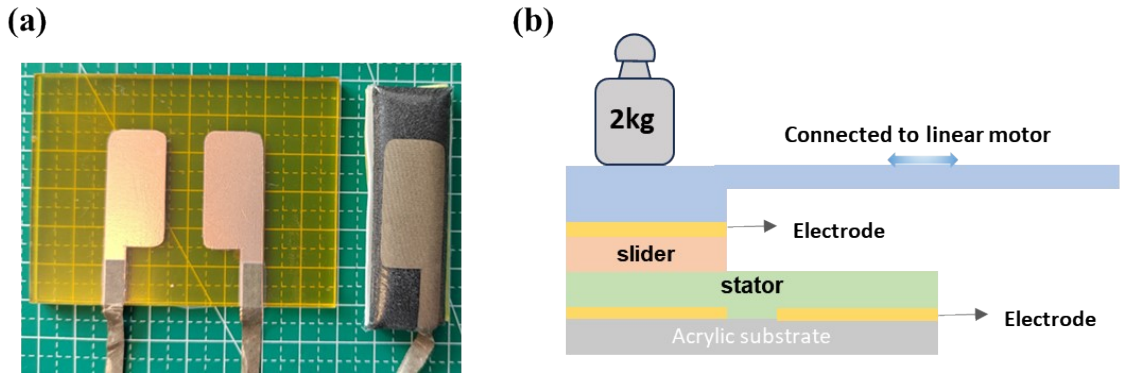

Supplementary Figure 1. (a) Optical photo of the fabricated SFT-TENG device (stator and slider). (b) Schematic diagram of the experimental setup.

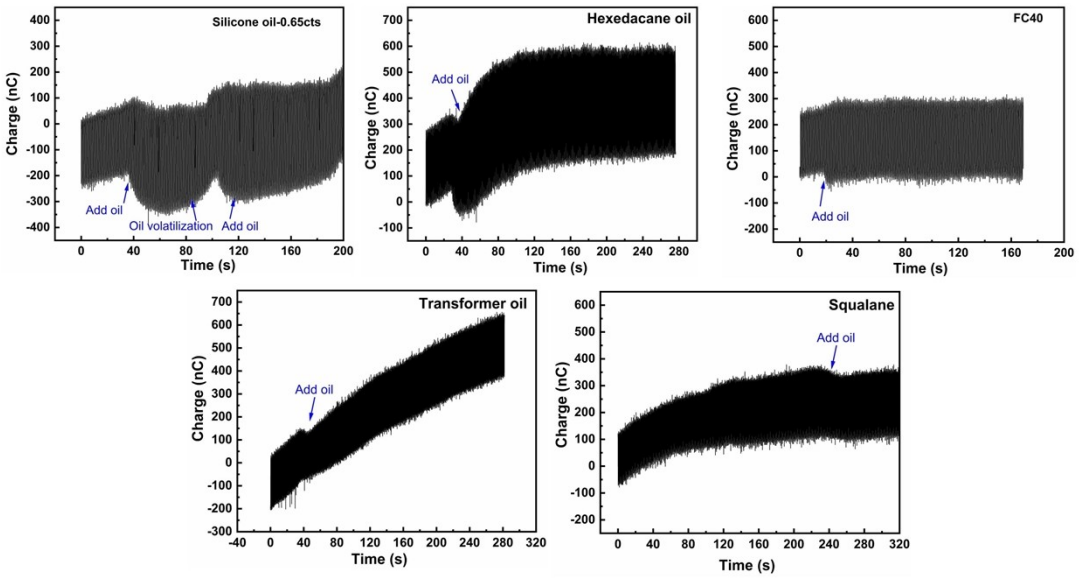

Supplementary Figure 2. Selection of insulating oil kind. Q_{sc} curve of SFT-TENG when adding different liquids oil onto friction surface.

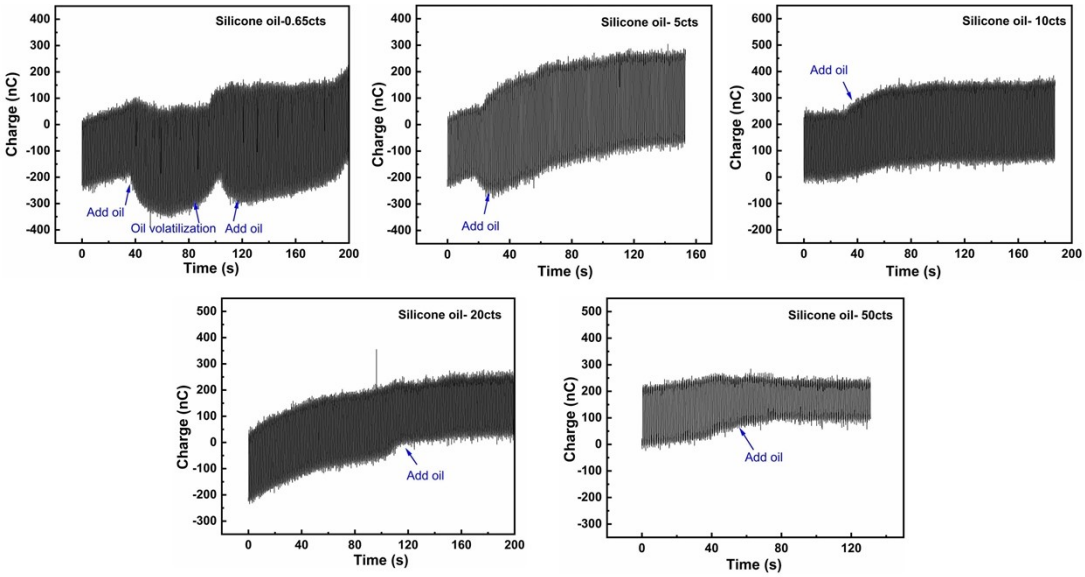

Supplementary Figure 3. Selection of silicon oil viscosity. (a) Q_{sc} curve of SFT-TENG when adding silicon oil with different viscosity onto friction surface.

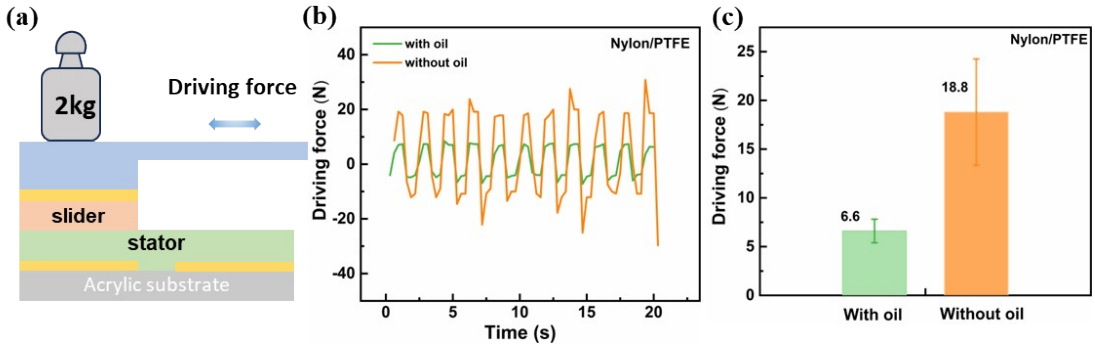

Supplementary Figure 4. Driving force of TENG under loading force of 20N. (a) Schematic of testing setup. (b) Dynamic force for driving the sliding part. (c) The statistics driving force of TENG in air and oil, respectively.

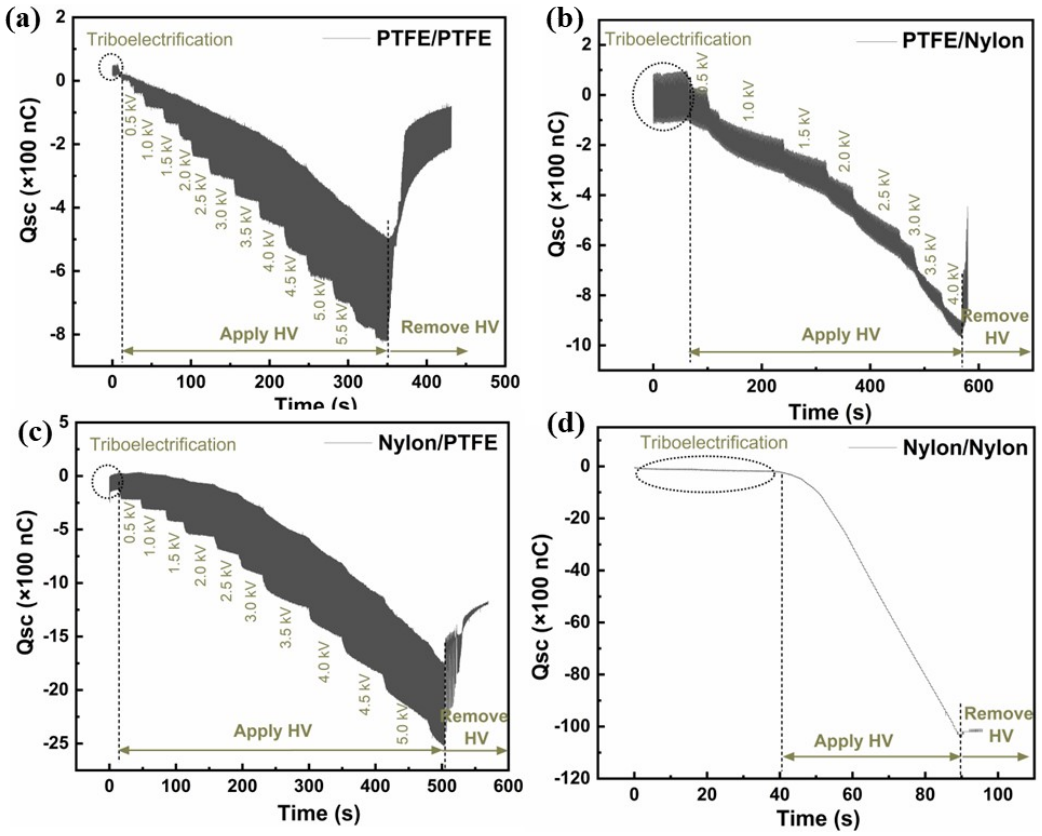

Supplementary Figure 5. The Q_{sc} curve of SFT-TENG under HV excitation with different combinations of Nylon and PTFE as slider and stator materials. (a) PTFE/PTFE pair, (b) Nylon/PTFE pair, (c) PTFE/Nylon pair, (d) Nylon/Nylon pair.

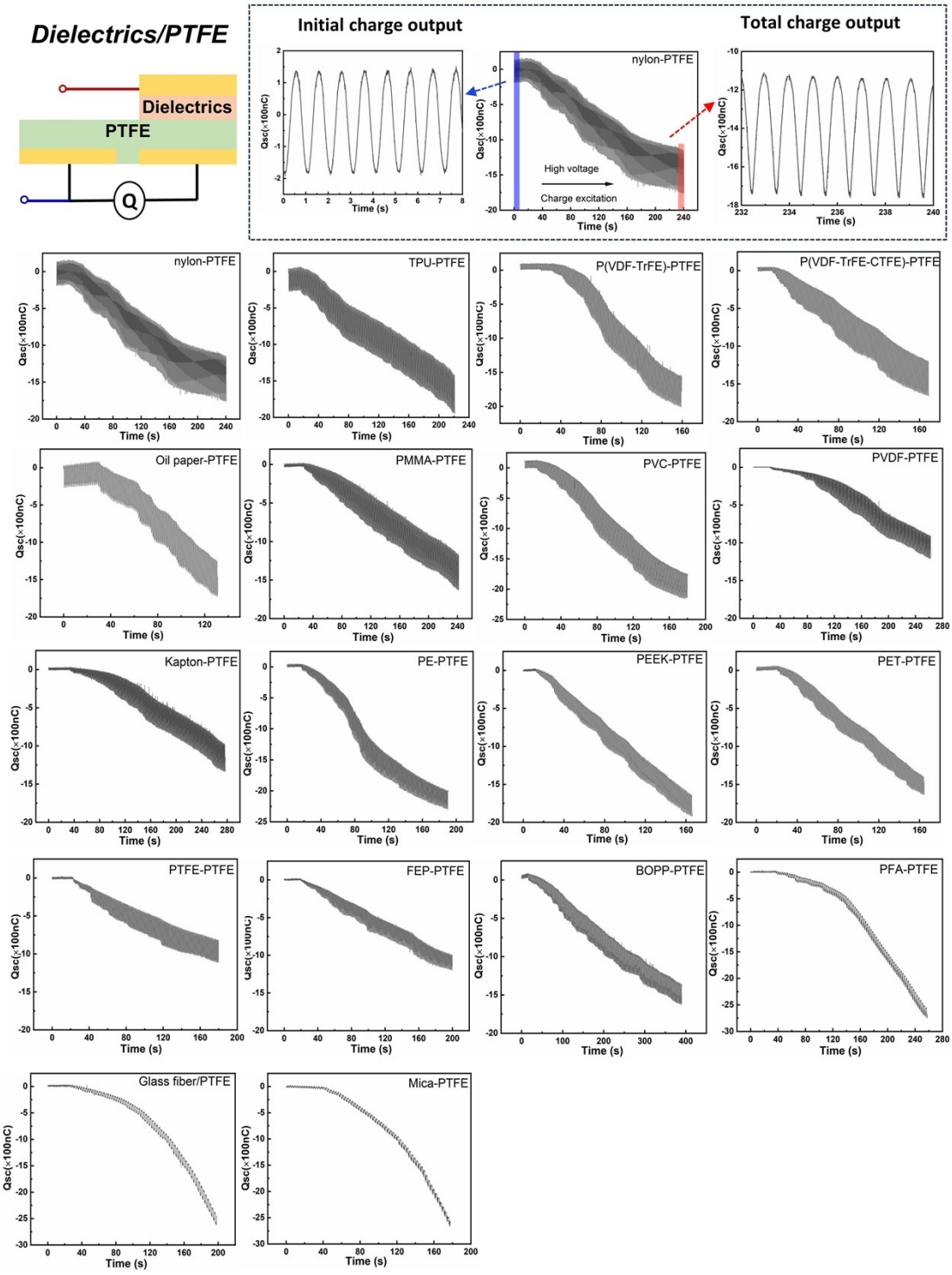

Supplementary Figure 6. Material selection of slider dielectric when using PTFE as the stator. The charge accumulation curve of SFT-TENG with different dielectric/PTFE pairs under high voltage.

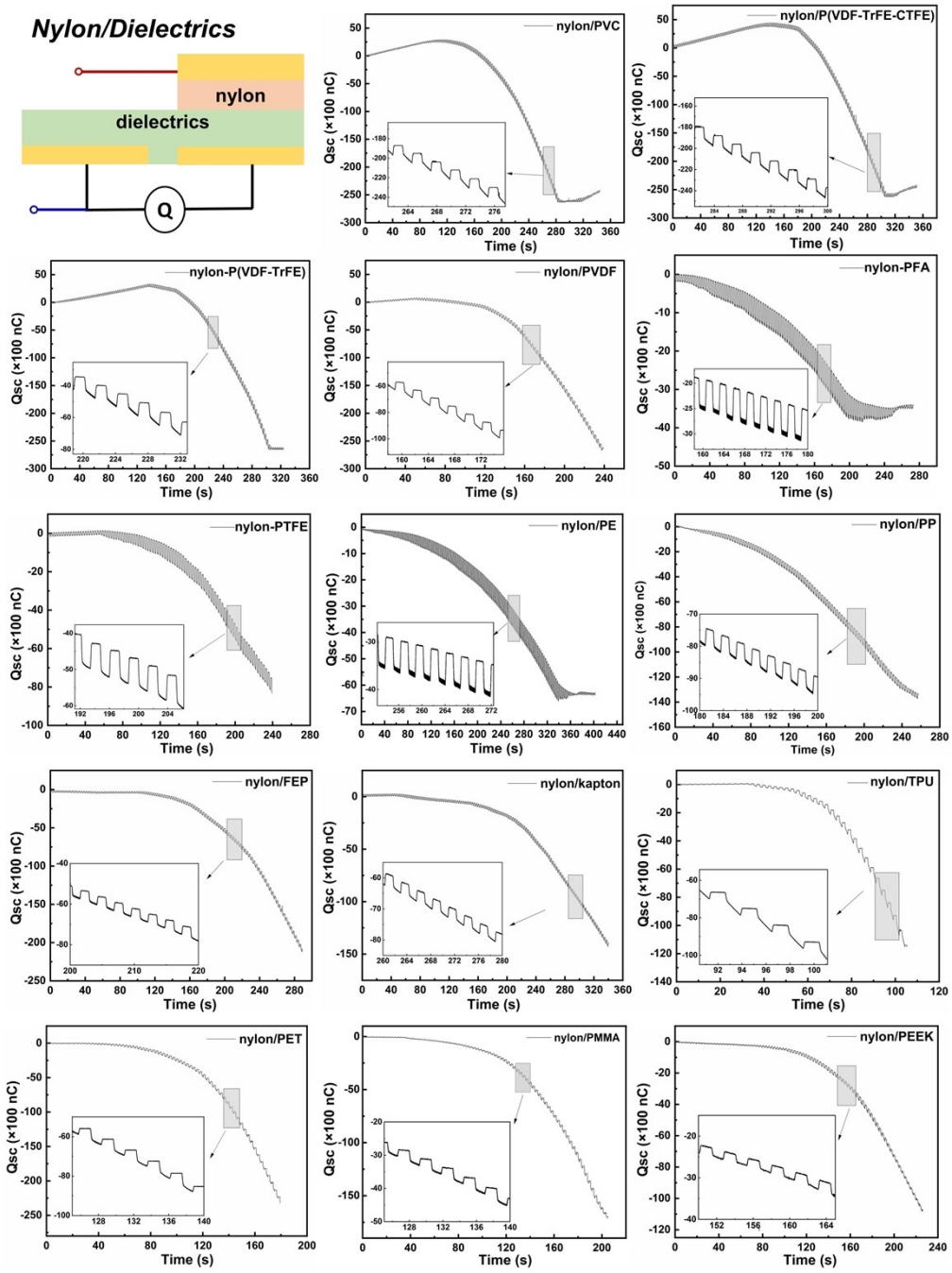

Supplementary Figure 7. Material selection of stator dielectric when using nylon as slider. The charge accumulation curve of SFT-TENG with different dielectric/PTFE pairs under high voltage. The drifting charge curve is observed due to the leakage current characteristic of different stator materials. The local enlarged charge curve is present in each inset figure to clearly show the details of output charge variation.

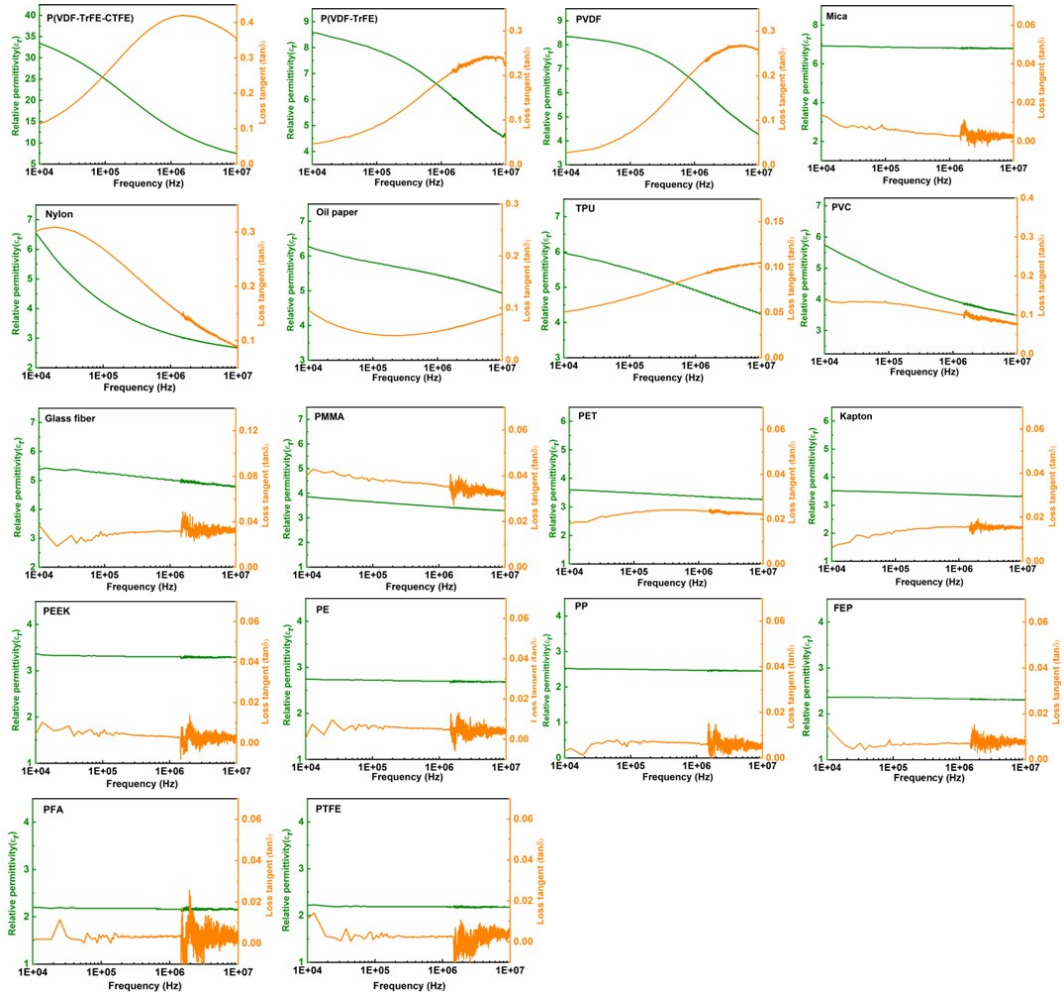

Supplementary Figure 8. Frequency dependence curve of relative permittivity (ε_r) and loss tangent (tan δ) for 18 kinds of tribomaterials used in SFT-TENG.

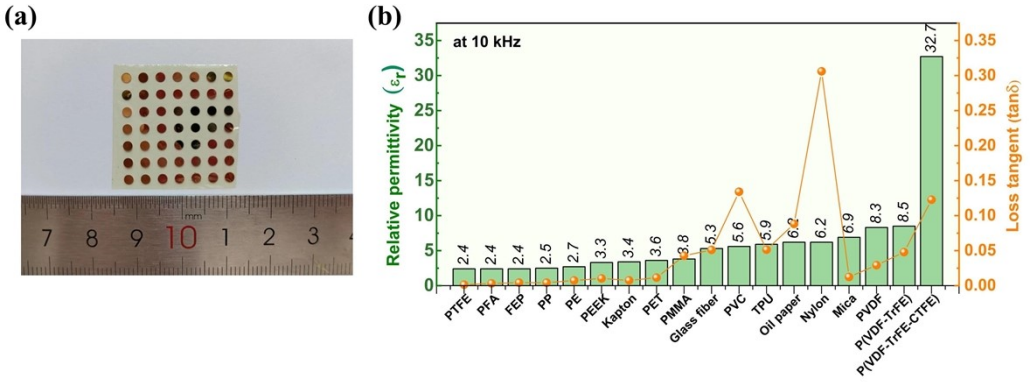

Supplementary Figure 9. (a) The tribomaterials film with sputtered gold electrode for electrical properties characterization. (b) Comparison of relative permittivity (ε_r) and loss tangent (tanδ) of tribomaterials at 10 kHz.

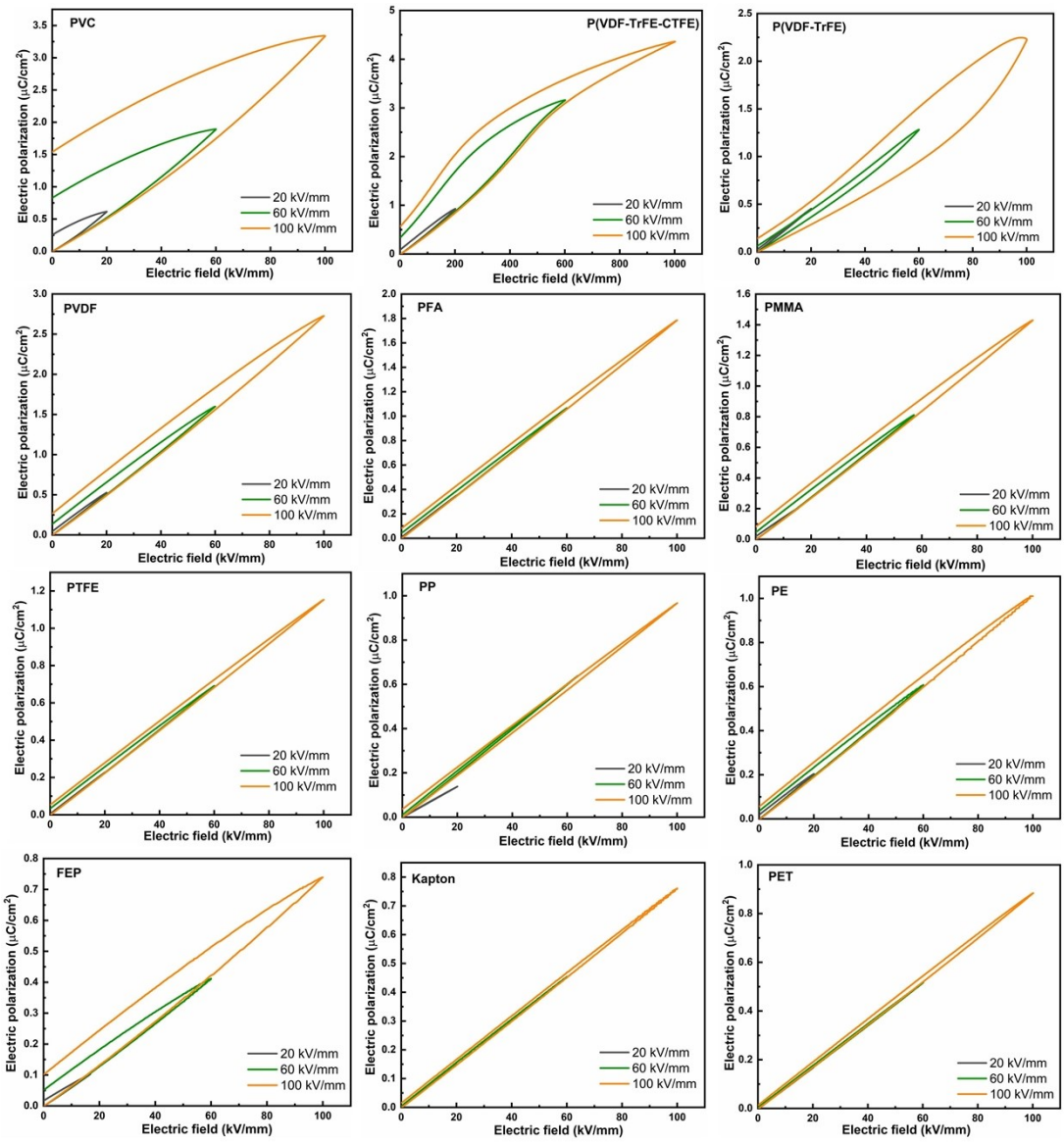

Supplementary Figure 10. The electric polarization hysteresis loops (*P-E* loop) of tribomaterials under high voltage.

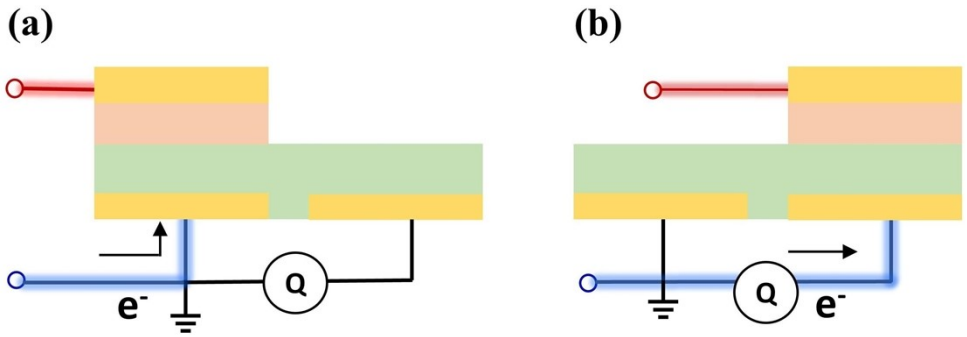

Supplementary Figure 11. The effect of external potential of high voltage source on the output circuit of TENG.

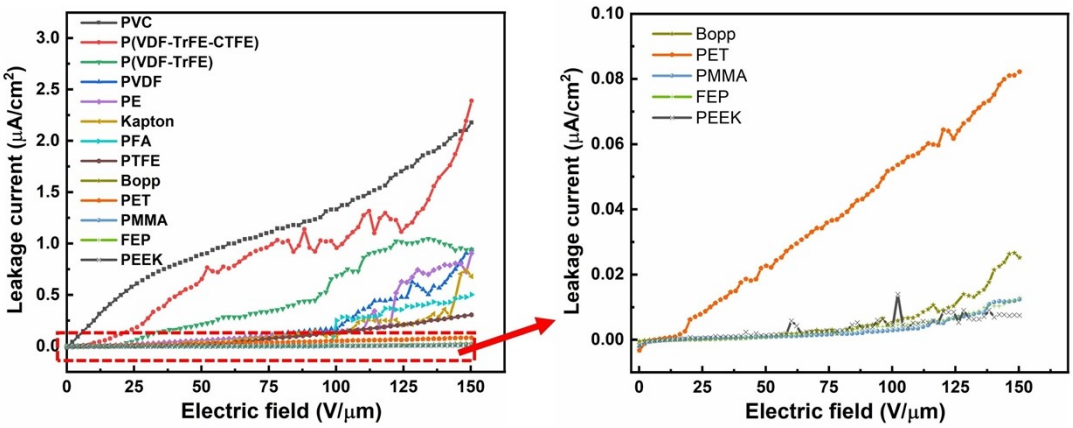

Supplementary Figure 12. The leakage current of tribomaterials under high voltage.

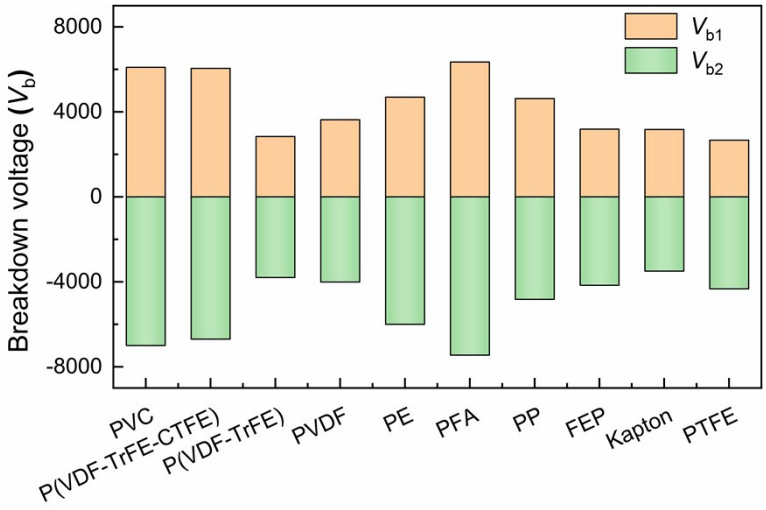

Supplementary Figure 13. The electric breakdown voltage (V_b) of SFT-TENG with different nylon/dielectrics pairs.

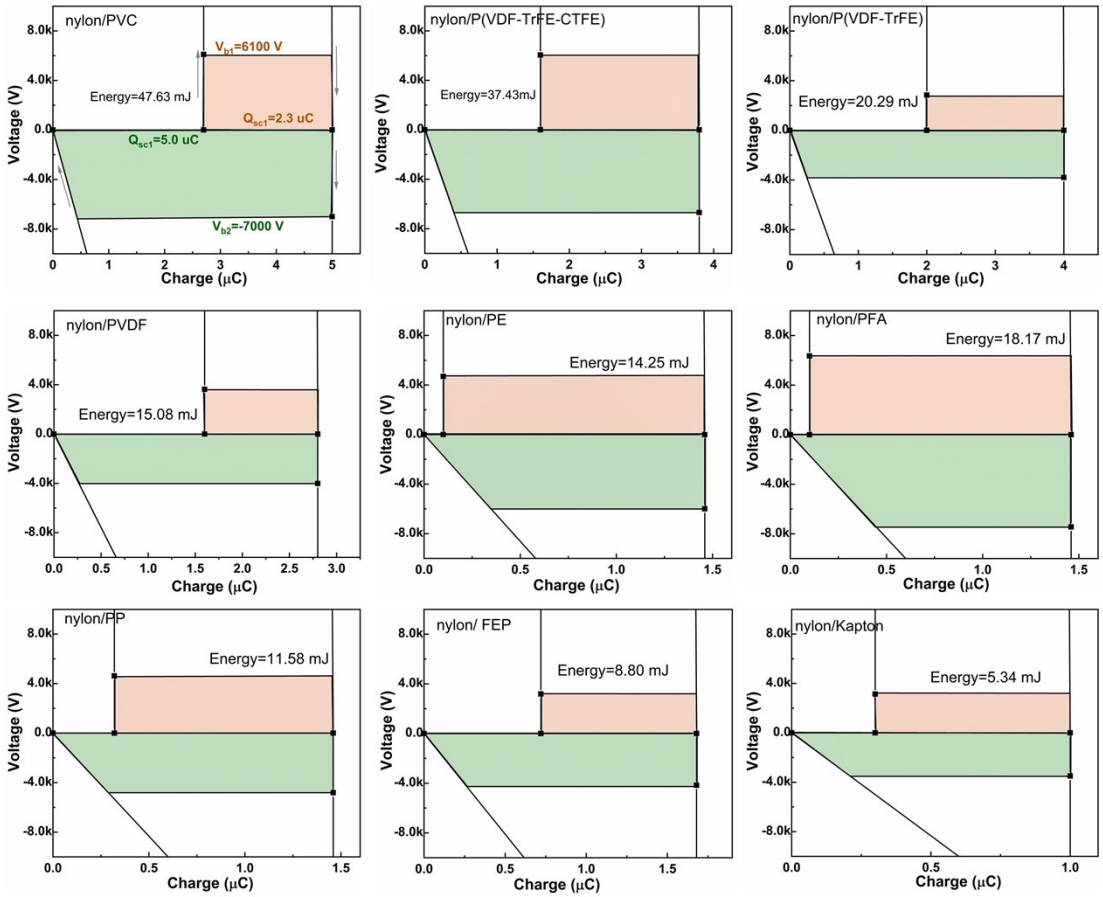

Supplementary Figure 14. The revised *V*-*Q* curve of SFT-TENG with nylon/dielectrics for the determination of maximized energy output.

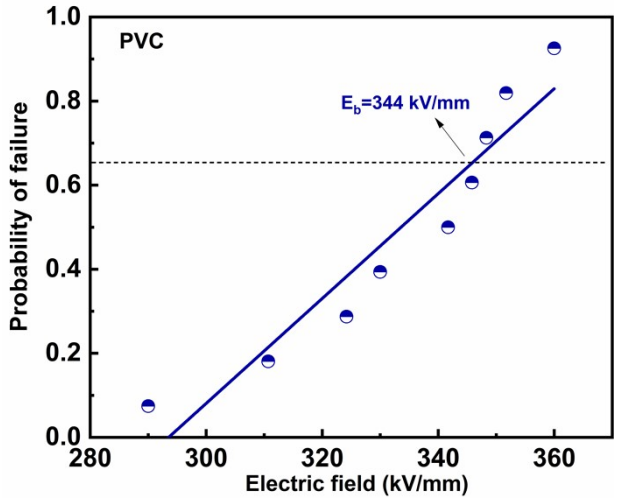

Supplementary Figure 15. The electric breakdown strength of PVC polymer measured by a dielectric voltage-withstand tests.

The electric breakdown strength of PVC polymer is a key parameter, which need to be given in COMSOL simulation for the judgment of breakdown point. Here it was measured by a dielectric voltage-withstand test. The DC voltage are exerted on the polymer with rising step of 500V until breakdown occurs. The breakdown voltage at this time devide by the polyer thickness is the electric breakdown field. The electric breakdown strength (E_b) is analyzed using a two-parameter weibull cumulative probability function:

$$P(E) = 1 - exp[-(E/E_b)^{\beta}] \quad (1)$$

where P(E) is the cumulative probability of failure occurring at the electric field lower or equal to E. The E_b is the scale parameter for experimental breakdown strength with a 63.2% probability for failure, and β is the shape parameter associated with linear regressive fit of the data distribution. The dielectric breakdown strength of PVC polymer is then extracted from a fit using Weibull failure statistics across 9 test samples.

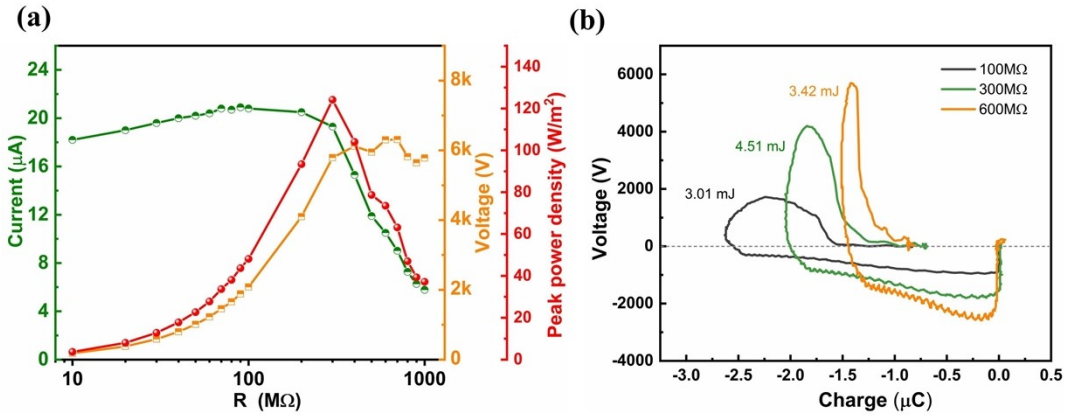

Supplementary Figure 16. The matching impendence and output peak power evaluation of SFT-TENG. (b) The *V*-*Q* curve of TENG under varied loads. The output current and voltage at different resistances from 10 MΩ to 1 GΩ are depicted. The maximum peak power density (P_{peak}) is 124.2 W/m^2 at a matching impedance of 300 MΩ. The output energy of TENG reaches 3.01 mJ, 4.51 mJ, and 3.42 mJ with an external load of 100M, 300 MΩ, and 600 MΩ, respectively.

Supplementary Table 1 The manufacturer of the different triboelectric materials

Material		Manufacture	Thickness (μm)
PTFE	Polytetrafluoroethylene	Shenzhen Chenguang Plastic Industry Co., Ltd, China	30
FEP	Fluorinated ethylene propylene	Guangzhou Jufu Plastic Industry Co., Ltd, China	20
PVC	Polyvinyl Chloride	Shenzhen Zhitong Material Technology Co., Ltd, China	38
PVDF	Poly (vinylidene fluoride)	home-made*	21
P(VDF-TrFE)	Poly (vinylidene fluoride-co-trifluoroethylene)	home-made*	20
P(VDF-TrFE-CTFE)	Poly(vinylidene fluoride-co-trifluoroethylene-co-chlorotrifluoroethylene)	home-made*	20
Kapton	Polyimide	Dongguan Innovative Electronic Materials Co., Ltd, China	22
PET	Polyethylene terephthalate	Dongguan Innovative Electronic Materials Co., Ltd, China	20
PMMA	Poly (methyl methacrylate)	home-made*	20
PE	Polyethylene	Shenzhen Meijianan Plastic Film Co., Ltd, China	30
PEEK	Polyetheretherketone	Shenzhen Meideyuan Plastic Industry Co., Ltd, China	25
PFA	Polyfluoroalkoxy	Shenzhen Chengnuoxin Plastic Industry Co., Ltd, China	50
PP	Polypropylene	Fujian Yongheng Plastic Industry Co., Ltd, China	25
Glass fiber	FR-4	Hongtaiyang Plastic Industry Co., Ltd, China	60
Oil paper	Nomex T410	Shenzhen Beizheng Insulation Industry Co., Ltd, China	20
Mica	-	Guangzhou Beilong Electronics Co., Ltd	28
Nylon	Polyamide	Dongguan Yuxin Plastic Industry Co., Ltd, China	25
TPU	Thermoplastic polyurethanes	Dongguan Jiaxin Plastic Industry Co., Ltd, China	23

*: The polymer films noted as “home-made” are fabricated by a common solution casting method due to not easy to be commercially purchased. The prepare process is present in Supplementary Note 2.

Supplementary Table 2 Parameters for the calculation of theoretical energy density for some commonly used tribomaterials

Dielectrics	ε_r	E_b (MV/m)	U_e (J/m^3)
PTFE	2.2	400	3.1×10^6
FEP	2.5	375	3.2×10^6
Kapton	3.4	314	2.7×10^6
PE	2.5	420	3.9×10^6
PVDF	8.0	430	1.3×10^7

Supplementary Table 3 Parameters for the simulation of electric potential and electric field distribution of the TENG in air and oil environments.

Mode parts	Size	Relative permittivity	Surface charge density
Slider layer（Nylon）	30×30×0.1 mm	6.2	233 uC/m^2
Stator layer (PVC)	70×30×0.1 mm	5.6	-100 uC/m^2
Electrode (Cu)	30×30×0.1 mm	-	-
Electrode gap	10×30×0.1 mm	5.6	-
Air	Surrounding environment	1	-
Oil	Surrounding environment	2.6	-

Supplementary Table 4 The parameters of geometrical physical model for COMSOL simulation

Mode parts	Size	Relative permittivity
Electrode (Cu)	30×30*0.1 mm	-
Stator dielectric layer (PVC)	70×30*0.1 mm	5.6
Slider layer（nylon）	30×30*0.1 mm	6.2
Electrode gap	10×30*0.1 mm	5.6
Air	Surrounding environment	1
Oil	Surrounding environment	2.6

Supplementary Table 5 The structure parameters and output performance comparison with the reported TENG

	Mode	Strategy	Electrode size	Dielectric material	Charge or charge density[3#] ($\mu C/m^2$)	Output voltage[3#]	Average power[2#]	Energy[1#]	Volume energy density (J/m^3)	Ref.
1	SFT (Rotary)	Floating self-excited	23.3 cm^2×12fans	25μm nylon; 30μm PTFE	71.5	470V (10 MΩ)	-	-	1222	[1]
2	SFT (Sliding)	Non-contact mode	3.5×7.5cm^2; Gap=3mm	50μm PTFE	260.15	3879V	-	-	14119	[2]
3	SFT (Sliding)	Self-excited liquid suspension	6.6×4.8cm^2; Gap=8mm	25μm nylon; 25μm nylon	704	4200V (1 GΩ)	-	-	54587	[3]
4	SFT (Sliding)	Charge space-accumulation effect	7.65×3.5 cm^2	25μm nylon; 50μm PTFE	1630	3000V (10GΩ)	-	-	25568	[4]
5	SFT (Sliding)	Interfacial lubrication and potential decentralizatio n design	2.1×5cm^2 Gap: 0.2cm	25μm nylon; 33μm PTFE	1960	2350V (10 GΩ)	-		70250	[5]
6	SFT (Rotary)	AC and DC coupling output	R-r: 8.4-1.5 cm	25μm nylon; 33μm PTFE	-	-	5.74 W/m^2 Hz (1Hz)	-	98965	[6]
7	SFT (Sliding)	Charge pumping with voltage stabilization and boosted current	7.5×10 cm^2	50μm PET; 50μm Kapton	1328	1400V (200 MΩ)	-	-	37100	[7]

8	SFT (Rotary)	Charge pumping	R-r: 22-3.5cm	50μm Kapton	-	-	78 mW (2Hz)	-	21051	[8]
9	SFT (Sliding)	Charge migration for volume effect	2×5 cm^2	1mm PU; 100μm FEP	-	3000V	-	1.2 mJ (1.2GΩ)	991	[9]
10	SFT (Sliding)	Hysteretic and ordered charge migration	R-r: 7.2-1.3cm	50μm FEP; 1mm PU	-	-	14.1 W/m^2 (1.5Hz)	-	8952	[10]
11	SFT (Sliding)	Charge leakage and ternary dielectric evaluation	25um PA; 50um PTFE		-	-	6.1 $W/(m^2 Hz)$	-	82000	[11]
12	CS	Charge-shuttling	10×10 cm^2	5μm PP	1850	-	1.4 mW, (1.7Hz)	-	16470	[12]
13	CS	High vacuum environments	3×3 cm^2	0.6cm BT; 200μm PTFE	1003	300V	50 W m^{-2}, (2Hz)	-	3472	[13]
14	CS	charge-excitation	10cm^2	50μm PTFE; 20μm Al	1250	800V (100 MΩ)	38.2 W/m^2 (4Hz)		9095	[14]
15	CS	Charge-excitation		4μm PEI	2380	1200V (100 MΩ)		287.6 mJ/m^2 (3MΩ)	71900	[15]
16	CS	Self-charge excitation with P(VDF-TrFE)	2×2 cm^2	9μm P(VDF-TrFE)	2200	1000V	40 W/m^2 (2.5 Hz)	-	4360	[16]

17	CS	Self-Polarization Effect	3×3 cm^2	7.5μm $BaTiO_3$/PVDF	1670	600V (100 MΩ)	-	44.736 J/m^3 (Distance 6mm)	268	[17]
18	CS	Polar high-k material	3×3 cm^2	7.5μm PZT+PVDF;	3530	500V (10 MΩ)	145.2 W/m^2 (4Hz)	-	36011	[18]
19	CS	Charge injection enabled by air breakdown	3×3 cm^2	30μm PTFE	880	650V (100 MΩ)	-	-	1110	[19]
20	CS	Water molecules induced self-polarization	2.5×2.5 cm^2	10μm P(VDF-TrFE)	2880	600V (100 MΩ)	-	-	3421	[20]
21	CS	Charge pumping	12×12 cm^2	5μm PP	1020	1000V (100 MΩ)	200 mW, (0.5 Hz)	-	27639	[21]
22	CS	charge trapping failure	2.5×2.5 cm^2	10μm CP/PVDF	4130	700V (10MΩ)	58.2 $W/(m^2 Hz)$ （4Hz）	-	57623	[22]
23	CS	charge reversion process	2.7×2.7 cm^2	30μm PI	780	-	-	190 mJ/m^2	6333	[23]

The evaluation method of maximized volume energy density is discussed in Supplementary Note 2.

Supplementary Note 1: The fabrication process of several home-made polymer films.

For the fabrication of PVDF, P(VDF-TrFE), and P(VDF-TrFE-CTFE) film, the raw powders were proportionally (10 wt.%) added in N, N-dimethylformamide solvent and stirred at 60℃ for 6h to form a stable and homogeneous solution. Then the solution was poured on a clear glass substrate followed by tape casting by a scraper with a clearance of 400um. After drying at 80℃ for 12h to volatilize the solvent, the polymer films with a thickness of ~20 μm were obtained to serve as tribomaterials for the TENG device.

For the fabrication of PMMA film, the raw powders were proportionally (20wt.%) added in N, N-dimethylformamide to the prepared solution. The tape casting using a scraper with a clearance of 300um to obtain films with a thickness of ~20 μm.

Supplementary Note 2: The preliminary test of SFT-TENG with different combinations of Nylon and PTFE as slider and stator materials, respectively.

The purpose of preliminarily testing in Supplementary Figure 5 is to explore the correlation between material properties and triboelectric/excitation charge output through different combinations of Nylon and PTFE as slider and stator materials, respectively. 1) Triboelectrification: Firstly, the triboelectrification reaches stability after several cycles of reciprocating sliding motion, shown as the initial curve part marked by a dashed circle, which represents only the triboelectric charge output. It can be observed that the tribomaterial pairs of Nylon/PTFE and PTFE/Nylon with large electronegativity difference show high triboelectric charges of ~200 nC compared with that of ~20 nC and ~10 nC for identical tribomaterial pairs of PTFT/PTFE and Nylon/Nylon. 2) Apply HV. Then, the positive and negative electrodes of the HV source are connected to the back electrode of the slider, and one of the bottom electrodes, respectively. Here, an external high voltage was applied to the TENG with an increasing step of 500V, while the corresponding Q_{sc} varies with voltage as shown in Supplementary Figure 5. For instance, the identical tribomaterial pair of PTFE/PTFE (as the slider/stator, respectively) achieves the Q_{sc} of 330 nC after experiencing the high voltage of 5000V, which mainly originated from the HV excitation. The TENG with Nylon/PTFE pair yields a much higher Q_{sc} of 700 nC due to the synergetic contributions from triboelectric charges and excitation charges. However, the TENG with PTFE/Nylon presents decreased Q_{sc} with the increased voltage step each time due to the competition between negative triboelectric charges from the slider PTFE and positive excitation charges. 3) Remove HV. Last, owing to

the high dielectric loss and leakage characteristics of Nylon, a very drifting charge curve is observed in the TENG with the Nylon/Nylon pair with almost no excitation effect.

Supplementary Note 3: Evaluation of maximized energy density for other reported work.

Although many research works have reported charge density or energy output performance of TENG, there are few direct numerical values on the maximized energy density. It is necessary to compare and analyze the detailed parameter from other literature to estimate their maximized energy density output capability. It should be noted that the calculation of the effective volume (V) is different for CS-TENG and SFT-TENG. For SFT-TENG, V is calculated as sliding area multiplied by the thickness of all stator and slider dielectrics layer. While for CS-TENG, it is given as electrode area multiplied by the sum of dielectrics layer thickness and separation distance. Here separation distance of 1 mm is assumed if not given clearly in the literature.

Here, three types of output parameters are considered to evaluate the maximized volume energy density. First, energy output (E) can be directly adopted to calculated U_{m} according to the equation (1)

$$U_m = E/V \tag{2}$$

Second, average power P_{ave} is used to calculate U_{m} referring to the equation (2)

$$U_m = P_{ave}/fV \tag{3}$$

where, f is working Frequency of TENG.

Third, charge (Q_{sc}) and maximum output voltage (V_{max}) are considered to imitate V-Q curve, so the E_{m} can be given as:

$$E_m = 2Q_{sc}V_{max}/V \tag{4}$$

Reference

1. Long L, et al. High performance floating self-excited sliding triboelectric nanogenerator for micro mechanical energy harvesting. Nature Communications 12, 4689 (2021).
2. Lei R, et al. Largely Enhanced Output of the Non-Contact Mode Triboelectric Nanogenerator via a Charge Excitation Based on a High Insulation Strategy. Advanced Energy Materials 12, 2201708 (2022).
3. He W, et al. Large Harvested Energy by Self-Excited Liquid Suspension Triboelectric Nanogenerator with Optimized Charge Transportation Behavior. Advanced Materials 35, 2209657 (2023).
4. Gao Y, et al. Achieving high-efficiency triboelectric nanogenerators by suppressing the electrostatic breakdown effect. Energy & Environmental Science 16, 2304-2315 (2023).
5. He W, et al. Ultrahigh Performance Triboelectric Nanogenerator Enabled by Charge Transmission in Interfacial Lubrication and Potential Decentralization Design. Research 2022.
6. He W, et al. Capturing Dissipation Charge in Charge Space Accumulation Area for Enhancing Output Performance of Sliding Triboelectric Nanogenerator. Advanced Energy Materials 12, 2201454 (2022).
7. Yang Z, et al. Charge Pumping for Sliding-mode Triboelectric Nanogenerator with Voltage Stabilization and Boosted Current. 11, 2101147 (2021).
8. Bai Y, et al. Charge Pumping Strategy for Rotation and Sliding Type Triboelectric Nanogenerators. Advanced Energy Materials 10, 2000605 (2020).

.

9. Fu S, et al. Conversion of Dielectric Surface Effect into Volume Effect for High Output Energy. Advanced Materials 35, 2302954 (2023).
10. Wu H, et al. A constant current triboelectric nanogenerator achieved by hysteretic and ordered charge migration in dielectric polymers. Energy & Environmental Science 16, 5144-5153 (2023).
11. Li Q, et al. Overall performance improvement of direct-current triboelectric nanogenerators by charge leakage and ternary dielectric evaluation. Energy & Environmental Science 16, 3514-3525 (2023).
12. Wang H, Xu L, Bai Y, Wang ZL. Pumping up the charge density of a triboelectric nanogenerator by charge-shuttling. Nature Communications 11, 4203 (2020).
13. Wang J, et al. Achieving ultrahigh triboelectric charge density for efficient energy harvesting. Nature Communications 8, 88 (2017).
14. Liu W, et al. Integrated charge excitation triboelectric nanogenerator. Nature Communications 10, 1426 (2019).
15. Liu Y, et al. Quantifying contact status and the air-breakdown model of charge-excitation triboelectric nanogenerators to maximize charge density. Nature Communications 11, 1599 (2020).
16. Li Y, et al. Improved Output Performance of Triboelectric Nanogenerator by Fast Accumulation Process of Surface Charges. Advanced Energy Materials 11, 2100050 (2021)

17. Wang J, et al. An Ultrafast Self-Polarization Effect in Barium Titanate Filled Poly(Vinylidene Fluoride) Composite Film Enabled by Self-Charge Excitation Triboelectric Nanogenerator. Advanced Functional Materials 32, 2204322 (2022).
18. Wu H, et al. Achieving Remarkable Charge Density via Self-Polarization of Polar High-k Material in a Charge-Excitation Triboelectric Nanogenerator. Advanced Materials 34, 2109918 (2022).
19. Wu H, et al. Improving and Quantifying Surface Charge Density via Charge Injection Enabled by Air Breakdown. Advanced Functional Materials 32, 2203884 (2022).
20. Wang J, et al. Enhancement of output charge density of TENG in high humidity by water molecules induced self-polarization effect on dielectric polymers. Nano Energy 104, 107916 (2022).
21. Xu L, Bu TZ, Yang XD, Zhang C, Wang ZL. Ultrahigh charge density realized by charge pumping at ambient conditions for triboelectric nanogenerators. Nano Energy 49, 625-633 (2018).
22. Wu H, et al. Ultrahigh output charge density achieved by charge trapping failure of dielectric polymers. Energy & Environmental Science 16, 2274-2283 (2023).
23. Guo Z, et al. Achieving a highly efficient triboelectric nanogenerator via a charge reversion process. Energy & Environmental Science 16, 5294-5304 (2023).